Parameter Analysis and Optimization of Layer Fidelity for Quantum Processor Benchmarking at Scale

Maria Jose Lozano Palacio, Hasan Nayfeh, Matthew Ware, and David C. McKay

IBM Quantum, IBM T.J. Watson Research Center, Yorktown Heights, New York 10598, USA

(Dated: October 19, 2025)

Abstract

With the continued scaling of quantum processors, holistic benchmarks are essential for extensively evaluating device performance. Layer fidelity is a benchmark well-suited to assessing processor performance at scale. Key advantages of this benchmark include its natural alignment with randomized benchmarking (RB) procedures, crosstalk awareness, fast measurements over large numbers of qubits, high signal-to-noise ratio, and fine-grained information [17]. In this work, we extend the analysis of the original layer fidelity manuscript to optimize parameters of the benchmark and extract deeper insights of its application. We present a robust protocol for identifying optimal qubit chains of length N, demonstrating that our method yields error per layered gate (EPLG) values 40%-70% lower than randomly selected chains. We further establish layer fidelity as an effective performance monitoring tool, capturing both edge-localized and device-wide degradation by tracking optimal chains of length 50 and 100, and fixed chains of length 100. Additionally, we refine error analysis by proposing parameter bounds on the number of randomizations and Clifford lengths used in direct RB fits, minimizing fit uncertainties. Finally, we analyze the impact of varying gate durations on layer fidelity measurements, showing that prolonged gate times leading to idling times significantly increase layered twoqubit (2Q) errors on Eagle R3 processors. Notably, we observe a 95% EPLG increase on a fixed chain in an Eagle R3 processor when some gate durations are extended by 65%. These findings extend the applicability of the layer fidelity benchmark and provide practical guidelines for optimizing quantum processor evaluations.

The development of quantum benchmarks allows for the evaluation and comparison of system performance across different devices and technologies. While average device performance is often inferred from randomized benchmarking (RB) protocols, these unstructured approaches do not necessarily reflect the layered or algorithmic nature of many near-term quantum workloads. Many near-term algorithms, such as the variational quantum eigensolver (VQE), the quantum approximate optimization algorithm (QAOA), and Trotterized dynamics, rely on the repeated execution of layered gate operations (see Ref. [5] for a review). Layered structures are also advantageous for other approaches: they connect naturally to Pauli learning and to error mitigation strategies that rely on rerunning circuits with different noise profiles [23, 7]. Together, these connections provide compelling motivation for benchmarks that evaluate performance in a layered framework.

Several benchmarking methods have since incorporated structured circuits—for example, quantum volume (QV) [4], cross-entropy benchmarking (XEB) [1], mirror RB [20], inverse-free (binary) RB [12], and clif-fordization [18]. These approaches provide valuable insights into overall device performance but offer limited fine-grained information about individual gate layers and typically require high-weight measurement out-

comes and extensive sampling, increasing overall runtime

Layer fidelity [17] directly addresses this gap by capturing the performance of large portions of a device while maintaining fine-grained access to individual gate errors. It measures the fidelity of a connected set of two-qubit (2Q) gates over N qubits by extracting gate errors using simultaneous direct RB [9, 21] in disjoint layers. In addition to its previously established advantages, layer fidelity aligns naturally with standard RB [16, 11] procedures, accounts for crosstalk effects, enables fast measurements across large numbers of qubits, and maintains a high signal-to-noise ratio. Given these benefits, further analysis is valuable to extract deeper insights into its applications. In this work, we extend the initial analysis in [17] by developing methods for identifying optimal qubit chains, establishing a stability monitoring tool, refining benchmark parameters, and analyzing the impact of varying 2Q gate durations.

In principle, layer fidelity can be measured for any connected set of qubits. However, prior work has shown that focusing on a one-dimensional chain offers practical advantages: it simplifies the partitioning of gates into disjoint layers while capturing crosstalk effects efficiently [17] . In many device geometries, such as the heavy-hex architecture, this makes a chain the natu-

^{*}mlozano@ibm.com

ral choice for benchmarking, requiring only two disjoint layers—one starting at Q0 (the even set) and another at Q1 (the odd set). Given the high number of possible subsets of N connected qubits, exhaustively evaluating all subsets quickly becomes infeasible for large-scale devices. For instance, a 127-qubit heavy-hex architecture, such as ibm_brisbane, contains 313,980 possible N = 100 qubit-long chains, while a 156-qubit heavy-hex device, such as ibm_marrakesh, has 35.804,119 such configurations. Due to this combinatorial complexity, heuristic methods are required to efficiently estimate the optimal layer fidelity over all possible subsets. In this work, we introduce a method for identifying the best qubit chains for N = 100 qubits on devices with 127, 133, and 156 qubits. This method can be generalized to any N, provided that a nonzero number of fully connected qubit chains of the desired length exists on the device.

Our approach for identifying the optimal chains uses single-qubit (1Q) and two-qubit (2Q) fidelities to prescreen and locate high-performing regions on a device. We employ two strategies, isolated and grid, which differ in the type of gate error data they utilize. Both approaches essentially rely on running characterization experiments prior to searching for the best N-qubit chain.

The isolated strategy extracts gate errors from isolated RB data, a variant of simultaneous RB [9] where all 2Q gate pairs are separated by at least two idle qubits and no barriers are enforced. In the worst case, obtaining all isolated gate errors would require O(N) experiments, but this number is lower in practice given the batching specified above. This setup naturally reduces some forms of crosstalk, such as ZZ interactions between coupled qubits in fixed architectures. Since isolated RB does not apply barriers, it also does not enforce the constraint of running layer fidelity at the maximal gate duration [17]. To account for this, we apply a small penalty to gate pairs with longer durations in the cost function defined in formula (1).

The grid strategy, in contrast, derives gate errors from layer fidelity RB, measured by running layer fidelity on a predefined grid of qubit chains (see Fig. 1 (c) and this notebook for an example). The grid consists of two sets of vertical and horizontal chains, ensuring that all 2Q gate pairs on the device are included. When a 2Q gate pair appears in both configurations, we take the average gate error. In a device with J couplers per qubit, these experiments can be grouped into O(J) batches, making the strategy scalable to larger devices. Layer fidelity RB is then used to identify high performing regions on a device and account for crosstalk. Simultaneous direct RB operations enforce the constraint that a timing barrier must be applied to all gates in a layer, leading to potential idle times for shorter gates. As such, a limitation of the grid strategy is that it can introduce length-dependent effects in a way that is not always representative of the final optimal 100-qubit chain. For example, the grid strategy will always run some grid chains at the maximal gate duration of the device, but there is no guarantee that the longest gate will be part of the optimal 100-qubit chain, so the length-dependent

effects this long gate introduces might not lead to the most accurate 2Q errors.

1 Protocol for finding the optimal 1D chain of N qubits

Once the 1Q and 2Q infidelities are obtained, both the isolated and grid strategies follow the same procedure to identify the highest-performing one-dimensional chain.

1. We define a cost function LF as the product of individual process fidelities F_j along some chain of size N

$$LF = \prod_{j} F_{j} \tag{1}$$

where $F_j = \frac{(1-\epsilon_j)(d+1)-1}{d}$ for all gate errors ϵ on the chain in question, and d=2 for 1Q errors and d=4 for 2Q errors.

The N-qubit chain with the highest cost function value among all possible candidates is designated as chain A.

- 2. To allow flexibility in chain selection, we identify additional candidates by selecting the next x chains with the highest cost function values. Here, x is an arbitrary number (defaulted to 15). This is important because, while chain A has the highest predicted performance, other chains with slightly lower cost function values may yield higher LF values when experimentally measured.
- 3. From this set of x chains, we choose two chains, B and C, that have the fewest overlapping qubits with chain A and have fairly trivial differences among them. Specifically, chain B is the chain that has the largest number of non-overlapping qubits relative to chain A, while chain C has the second largest. This produces a total of three chains.
- 4. Since we are using two strategies, the isolated strategy and the grid strategy, we must apply this procedure twice. That is, we must find the best three estimated chains for each of the two methods. This leads to a final set S = [A, B, C, D, E, F], where A, B, and C come from the grid strategy, and D, E, and F come from the isolated strategy. Here, chain A represents the optimal chain identified by the grid strategy, while chain D is the optimal chain identified by the isolated strategy.
- 5. We then run layer fidelity on all chains in set S and compare their performance. The best N-qubit chain for the device is defined as the chain within set S that exhibits the lowest average error per layered gate (EPLG) value, where

$$EPLG = \frac{4}{5}(1 - LF^{N-1}) \tag{2}$$

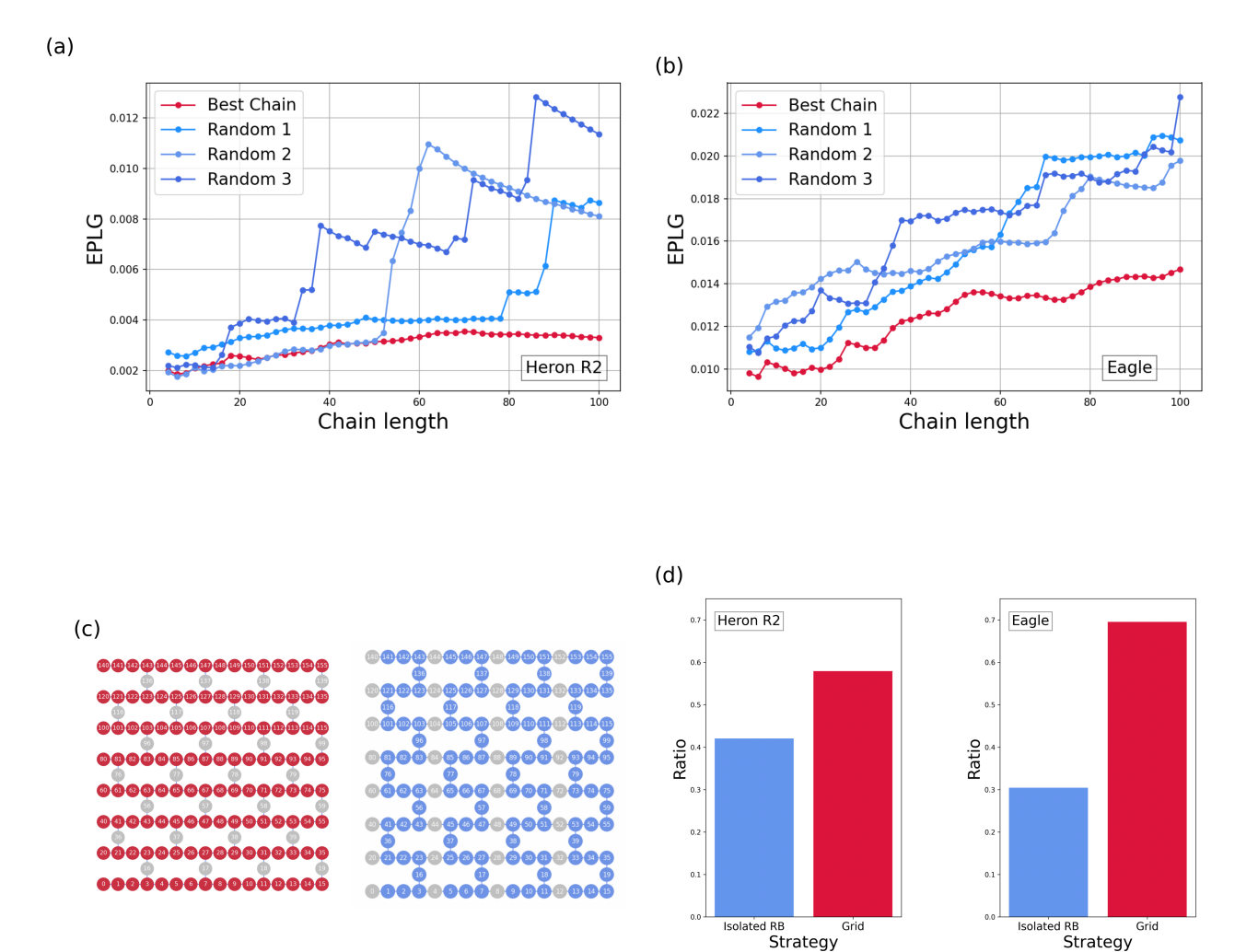


Figure 1: (a) EPLG vs chain length for the optimal N-qubit chain (red) and 3 random chains (blue) on $ibm_marrakesh$ (Heron R2). The lowest EPLG corresponds to the optimal chain, with 3.2×10^{-3} , followed by a random chain with 8×10^{-3} . (b) EPLG vs chain length for the optimal N-qubit chain (red) and 3 random chains (blue) on $ibm_brisbane$ (Eagle R3). The lowest EPLG corresponds to the optimal chain, with 1.4×10^{-2} , followed by a random chain with 1.9×10^{-2} . (c) Horizontal grid configuration (red) and vertical grid configuration (blue) for a Heron R2 processor. (d) Frequency of occurrence of the optimal chain (isolated RB strategy (blue) vs grid strategy (red)) for a Heron R2 (left) and Eagle R3 (right). Red has a 60% occurrence percentage for Heron R2 and a 70% occurrence percentage for Eagle R3.

A key test of our protocol is whether it outperforms a randomly selected chain. To evaluate this, we compare the best N-qubit chain identified by our method to three randomly selected N qubit chains on two devices: $ibm_marrakesh$ (Heron R2, 156 qubits) and $ibm_brisbane$ (Eagle R3, 127 qubits). The results demonstrate a clear advantage of the proposed method, as the estimated best chains significantly outperformed their random counterparts. Specifically, the best chains identified by our protocol measured EPLG values of 3.2×10^{-3} for $ibm_marrakesh$ and 1.4×10^{-2} for $ibm_brisbane$, 70% and 40% lower than the best performing random chains, respectively (see Fig. 1 (a) and (b)).

In addition to comparing against random chains, we also examine the relative performance of the grid and isolated strategies. We count the frequencies of occurence for each chain and strategy and normalize them by the total counts. By construction, one might expect chain A, selected by the grid strategy, to consistently

yield the lowest EPLG within set S. However, a detailed comparison of the EPLG of chain A against those of chains B, C, D, E, and F reveals that the highestperforming chain can originate from other candidates in the set as well. Daily data collected over 104 days shows that on Eagle R3 processors, the grid strategy identified the best-performing chain in 70% of cases, with chain Aexhibiting the lowest EPLG in half of those instances. On Heron processors, the performance of both strategies was more evenly distributed: the grid strategy identified the best-performing chain in 60% of cases, with chain A exhibiting the lowest EPLG in a third of those cases (see Fig. 1 (d)). These results align with expectations. The grid strategy, which accounts for crosstalk through layer fidelity RB, makes more accurate predictions on Eagle R3 processors, where crosstalk is significant. On Heron processors, however, performance for both strategies is similar, since the tunable coupling architecture reduces crosstalk [8].

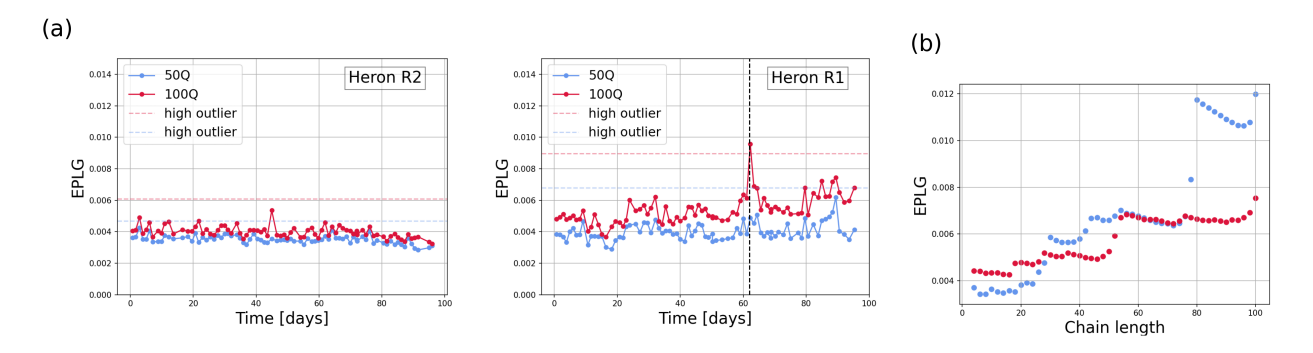


Figure 2: (a) EPLG vs time for ibm_fez (Heron R2, left) and ibm_torino (Heron R1, right) for chains of length 50 (blue) and 100 (red). Dashed lines indicate the high outlier region over the most recent 15 days. On day 62, the EPLG of the 100-qubit chain on ibm_torino increases to 1.2×10^{-2} . (b) EPLG vs chain length for ibm_torino on day 62 (blue) and day 65 (red). On day 62, there are two 2Q gates at lengths 78 and 79 with poor fidelities due to a TLS interaction involving the qubits in those gates. EPLG recovers by day 65.

2 Using EPLG to track device stability over time

Assessing a device's reliability requires tracking performance over extended periods of time. EPLG serves as a meaningful stability metric, as it reflects the ability to execute long circuits relevant to utility-scale applications. By monitoring EPLG over time, we can detect fluctuations in system performance and identify potential degradations.

To evaluate stability, we consider two complementary cases. The first analyzes EPLG for the optimal chain identified at the time of each layer fidelity run, providing insight into how the best-performing regions of a device evolve. The second focuses on EPLG for a fixed chain, highlighting the long-term stability of a specific region.

In the first case, we run layer fidelity once per day over a 100-day period, recording EPLG values for the best N=100 and M=50 qubit-long chains on a device. The long N-qubit chain is determined using the optimal chain-finding method described in Section 1, while the short M-qubit chain is the subset within the N-qubit chain that has the lowest EPLG value for length M. That is, it's the subchain with the highest product of process fidelities across 50 connected qubits from all measured fidelities on the 100 qubit-long chain. To detect sudden performance degradation, we define a high outlier threshold as $T=Q_3+1.5\times IQR$ over a rolling 15-day window, where Q_3 is the third quartile, Q_1 is the first quartile, and $IQR=Q_3-Q_1$.

This approach captures two types of performance degradation. The M-qubit chain reflects device-wide performance declines, while the N-qubit chain detects localized degradation in specific gate pairs. Since longer chains inherently include more gate pairs, it is harder to avoid low-performing gates as N approaches the device size. Thus, an EPLG increase in the N-qubit chain likely indicates an issue with a specific gate pair. In contrast, an EPLG increase in the M-qubit chain suggests a broader degradation affecting most gate errors.

We analyze stability on two Heron devices: ibm_torino (R1, 133 qubits) and ibm_fez (R2, 156 qubits). Heron R2 differs from R1 in two main respects: it increases the qubit count from 133 to 156, yielding more candidate N- and M-qubit chains, and it incorporates a two-level system (TLS) mitigation mechanism not present in R1 [10].

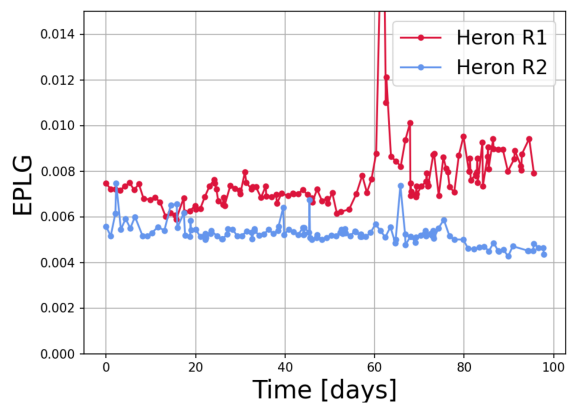
On both devices, EPLG remains stable for the M-qubit chain, with no significant fluctuations during the 100-day period. The EPLG median value on ibm_fez (R2) lies at 4.3×10^{-3} , while that of ibm_torino (R1) lies at 4.9×10^{-3} . Both standard deviations σ_f and σ_t are in the order of 10^{-4} .

When scaling to longer N-qubit chains, ibm_fez maintains stable EPLG values around a median of 4.9×10^{-3} , whereas ibm_torino exhibits oscillations mainly between 5.4×10^{-3} and $7.6 \times , 10^{-3}$, with some notable values as high as 1.2×10^{-2} (see Fig. 2 (a)). During this 100-day period, the absolute difference between the lowest and highest EPLG for an optimal N-qubit chain in ibm_torino is 7.4×10^{-3} . On the other hand, ibm_fez shows an absolute difference almost three times smaller, namely 2.6×10^{-3} . This difference in stability can also be seen from the standard deviation in the data. While σ_f remains in the order of 10^{-4} , σ_t rises to 10^{-3} .

A notable event occurs on day 62, where ibm_torino shows a sudden EPLG spike to 1.2×10^{-2} . This anomaly is traced to two specific 2Q gate pairs within the N-qubit chain used that day. Further analysis revealed that two qubits involved in those gates were interacting with a TLS during this time frame. TLS defects are known to significantly impact qubit coherence [6] [19] [2] and gate errors [14] [15], and this effect is directly captured by the layer fidelity benchmark. The fidelity of the associated 2Q gates recovers by day 65 and EPLG goes back to a stable value of 7.5×10^{-3} for N=100 (see Fig. 2 (b)).

We observe similar stability trends for the best Nand M-qubit chains across other Heron R2 devices, such as $ibm_marrakesh$, where both chain lengths exhibit stable EPLG values. These findings could suggest that





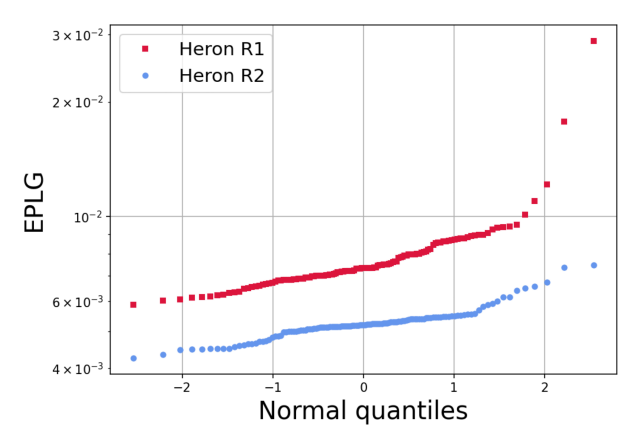


Figure 3: (a) EPLG vs time for ibm_fez (Heron R2, blue) and ibm_torino (Heron R1, red) for a fixed chain of length N=100. On day 62, the EPLG of ibm_torino increases to 2.8×10^{-2} due to a strong TLS interaction involving one qubit in the chain. (b) Normal quantile distribution of EPLG values over a 100-day period for fixed chains on ibm_fez (Heron R2, blue) and ibm_torino (Heron R1, red).

(b)

the additional TLS mitigation mechanisms in Heron R2 devices [10] contribute to this improved stability, though it's possible that having a larger number of candidate chains from an increased qubit count could also result in more stable chains to choose from.

We next consider the stability of a fixed N = 100qubit chain on Heron R1 and R2 devices. To do this, on each device, we start with a chain identified as the optimal chain at time t = 0 and track its EPLG variation over the subsequent 100-day period. In this experiment, we did not measure the EPLG of these chains directly; instead, we reconstructed it from historical data containing the process fidelities of all 2Q gates on each device, obtained using the grid method described earlier. The final EPLG values were then computed using Eqs. (1) and (2). This serves as a reliable approximation, as Heron devices exhibit negligible crosstalk [17]. As expected, *ibm_torino* shows larger EPLG oscillations than ibm_fez . The absolute difference for ibm_torino is 2.3×10^{-2} , while that of ibm_fez is 3.2×10^{-3} , an order of magnitude smaller. A similar trend is visible in the standard deviation, with $\sigma_t \approx 10^{-3}$ and $\sigma_f \approx 10^{-4}$ (see Fig. 3 (a)).

The same TLS-related event that affected the optimal chain of ibm_torino on day 62 also impacts the fixed chain. One gate in the fixed chain strongly interacted with a TLS on this day, which is clearly reflected in the 2.8×10^{-2} EPLG spike in Fig. 3 (a). Examining the normal quantile distribution of EPLG values over the 100-day period, the most pronounced difference between R1 and R2 devices appears in the third quantile, where the values of ibm_torino deviate from the linear trend observed elsewhere (Fig. 3 (b)).

Overall, while both devices maintain stable performance for shorter chains, ibm_fez , a Hero R2 processor, demonstrates markedly improved stability when scaling to long N-qubit chains. By capturing both gradual trends and isolated anomalies, layer fidelity provides a direct and scalable means of quantifying device stability, offering a valuable tool for assessing the long-term reliability of large-scale quantum processors.

3 Assessing EPLG variation from direct RB fits

The stability analysis demonstrates that EPLG is a reliable metric for tracking performance. However, its accuracy is influenced by the quality of RB decay fits, which depend on parameters such as number of randomizations and Clifford lengths. To ensure reliable EPLG estimates, we investigate how these factors affect fit precision and establish reasonable lower bounds for minimizing uncertainties.

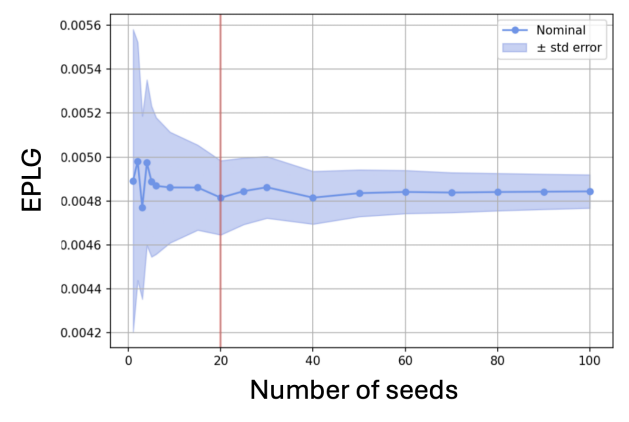
To achieve this, we collect data from 100 randomizations for each gate in a fixed N=100 qubitlong chain. The data is obtained from 10 consecutive layer fidelity runs on a fixed chain on ibm_fez (Heron R2), with each run consisting of 10 randomizations, 200 shots per circuit, and Clifford lengths C=[1,30,40,60,80,100,150,200,300,400,500,600]. All circuits are generated using Qiskit and executed via the IBM Quantum cloud interface (see this notebook for running layer fidelity on a fixed chain).

To estimate the decay rate α , we randomly sample data from r randomizations and fit them to $P_1 = a \times \alpha^x + b$. Here, we consider all Clifford lengths in C. We then take the nominal fit values, along with upper and lower bounds defined by the standard error. Using these three values, we estimate 1Q and 2Q process fidelities according to $F_j = \frac{1+(d^2-1)\alpha}{d^2}$ where d=4 for 2Q gates and d=2 for 1Q gates. Finally, we compute layer fidelity as described in the original manuscript [17] and normalize it to EPLG according to equation (2).

In a separate analysis, we repeat this process while varying the number of Clifford points by excluding certain lengths in C, and fixing the number of randomizations to r=10.

Results are shown in Fig. 4. The left figure presents EPLG as a function of r randomizations for the nominal fit, along with the upper and lower bounds obtained by propagating the standard error in the RB decay fits. The data reveals a clear asymptote at 4.8×10^{-3} with





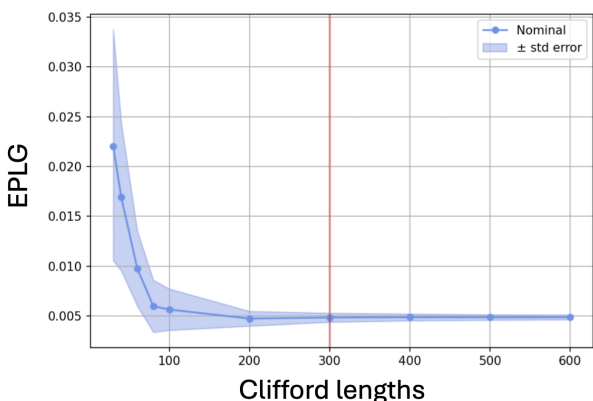


Figure 4: (a) EPLG vs number of randomizations on ibm_fez (Heron R2) for a chain of length 100. Shaded areas denote the standard error, propagated from error fits in RB decay. Nominal EPLG starts stabilizing at around r = 6. Shaded EPLG areas start stabilizing at around r = 20. (b) EPLG vs Clifford lengths on ibm_fez for a chain of length 100. Shaded areas denote the standard error, propagated from error fits in RB decay. Nominal EPLG starts stabilizing at around 100 Cliffords. Shaded EPLG areas start stabilizing at around 300 Cliffords.

uncertainties ranging from $\pm 9.3 \times 10^{-4}$ for r=1 to $\pm 9.4 \times 10^{-5}$ for r=100. As expected, EPLG variation is largest for small values of r but its nominal value stabilizes rapidly for $r \geq 6$. The upper and lower bounds start to stabilize around $r \geq 20$, serving as reasonable lower bounds for the number of randomizations.

The right figure further illustrates EPLG as a function of c Cliffords, obtained by excluding specific lengths from C and refitting. The data shows that the nominal EPLG value stabilizes at around c=100, with a clear asymptote at 5×10^{-3} . Uncertainties range from $\pm 1.1\times 10^{-2}$ to 2.4×10^{-4} and are largest when using fewer Clifford lengths (e.g., <300), but they quickly converge with more Cliffords. For this level of EPLG, convergence is achieved with at least 300 Cliffords, with a total of 9 points distributed between 1 and 300. We note that if the nominal EPLG were to change significantly, a larger number of Clifford lengths would be required to achieve comparable convergence.

4 Analyzing the impact of varying gate lengths on layer fidelity

While optimizing RB decay fits reduces EPLG uncertainty, other factors also influence layer fidelity results—one key constraint is gate duration. On Eagle processors, the fixed coupling architecture imposes stricter constraints on frequency collisions, which often require lengthening certain 2Q gates. In addition, the cross-resonance interaction is highly sensitive to qubit detuning [3, 22, 13]; when qubits lie in a poor detuning regime, gates must be extended to achieve sufficient entangling interaction. Layer fidelity explicitly enforces barriers at the 2Q gate layer, so all preceding gates must complete before the circuit advances. This mirrors the scheduling used in practical algorithms [14], where layered operations cannot begin until the prior

layer is finished. Consequently, the effect of lengthened gates is directly reflected in the benchmark, faithfully capturing the timing constraints of real algorithm execution. At the same time, however, enforcing barriers also introduces idle periods for shorter gates in the protocol [17], making it important to examine how this constraint influences the results.

We compare three distributions of 2Q gate errors on two devices that have varying 2Q gate durations: $ibm_marrakesh$ (Heron R2, median duration 68ns, max 80ns) and $ibm_sherbrooke$ (Eagle R3, median duration 533ns, max 881ns). These error distributions are taken from a chain of the form shown in Fig. 5 (b) and are derived from:

- 1. **Isolated RB**: A variant of simultaneous RB where 2Q gates are spaced apart by at least two idle qubits. No barriers are applied.
- 2. Isolated RB (with a delay): Same as (1), but each 2Q gate is followed by an additional delay such that the total duration of the layer equals the maximum gate duration in that disjoint layer. This captures length-dependent effects but not crosstalk.
- 3. Layer Fidelity RB: Simultaneous RB as described in the layer fidelity protocol. This applies barriers and engages all gates in the current disjoint layer. This captures both crosstalk and length-dependent effects.

Previous work has shown that 2Q gate error distributions are tighter on Herons than on Eagles when considering crosstalk and equal gate durations [17]. Here, we extend this analysis to include longer gate durations.

We measure all 2Q gate errors on $ibm_marrakesh$ and $ibm_sherbrooke$ with the methods described above and analyze their distributions using normal quantile plots. In both cases, median errors are lowest for isolated RB, followed by the isolated RB with delay and then layered RB.

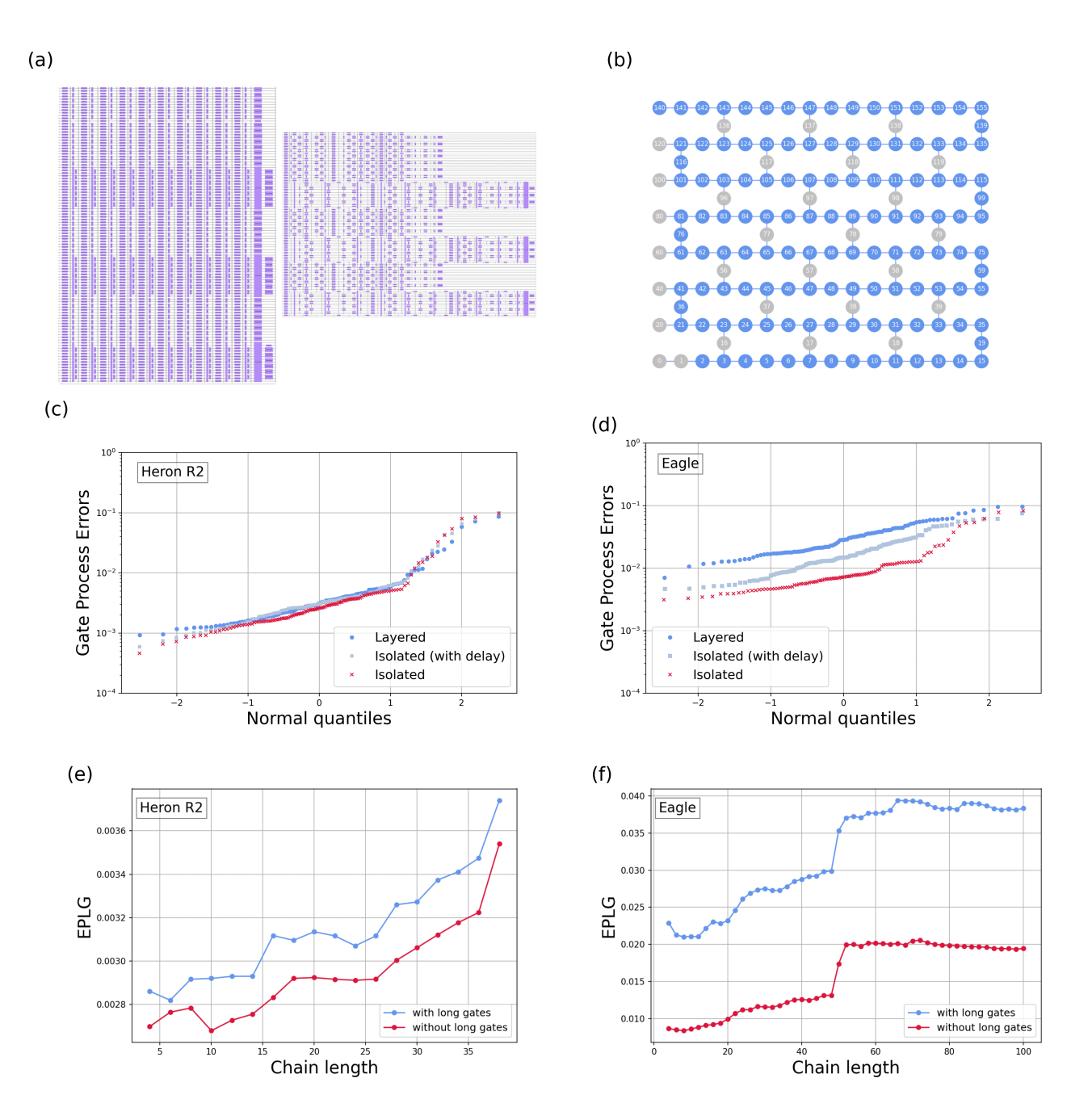


Figure 5: (a) Layered RB (left) and isolated RB (right) circuits. Layered circuits contain an alignment barrier, unlike the isolated case. Isolated RB with a delay, not picture here, looks similar to the layered case, except that it has a separation of 2 idle qubits between 2Q gates. (b) Chain used to measure 2Q errors on $ibm_marrakesh$. The chain for $ibm_shebrooke$ is similar. (c) 2Q error distributions for $ibm_marrakesh$. (Heron R2). Blue line is layered RB including long gates, light blue line is isolated RB with a delay, and red line is isolated RB. Distributions are fairly tight. (d) 2Q error distributions for $ibm_sherbrooke$ (Eagle R3). The ratio between the median 2Q error of layered RB and isolated RB is 3.9x, while the ratio between isolated RB with and without a delay is 2x. (e) EPLG vs chain length for $ibm_marrakesh$ for a fixed chain with 6 gates of varying gate lengths. Blue line corresponds to layer fidelity run on all gates at the maximal gate length of 80ns (3.68×10^{-3}) . Red line excludes all 6 gates with longer durations, and runs the rest at their corresponding duration of 68ns (3.55×10^{-3}) . (f) EPLG vs chain length for $ibm_sherbrooke$ for a fixed chain with 7 gates of varying gate lengths. Blue line corresponds to layer fidelity run on all gates at the maximal gate length of 881ns (3.7×10^{-2}) . Red line excludes all 7 gates with longer durations, and runs the rest at their corresponding duration of 533ns (1.9×10^{-2}) .

On *ibm_marrakesh*, the differences in median 2Q errors across these distributions are small (see Fig. 5 (c)). On this device, 22 out of 176 gates have a dura-

tion 17% longer than the median. Our data shows that lengthening the duration of some 2Q gates has little impact on layered RB outcomes.

On $ibm_sherbrooke$, the effect is more pronounced. On this device, only a small fraction of gates exceed the median duration (7 out of 144 gates), but the longest gates are 65% longer. We observe that the median 2Q layered error is 3.9x higher than the isolated case without a delay, while the median isolated RB case with a delay is 2x higher than the case without it. As expected, our results confirm the intuition that imposing a longer gate duration on layered RB significantly increases errors on this device.

To directly assess the impact of longer gate durations on EPLG, we select a fixed N = 100 qubitlong chain with varying gate durations and run two instances of layer fidelity—one with all gate durations included and another with long gates removed. the latter case, we predict the layer fidelity value at a length of 100 by re-introducing the process fidelities of the removed gates from the layered RB case described above. The N-qubit chain we select on ibm_marrakesh contains 7 long gates, while the Nqubit chain we select on *ibm_sherbrooke* contains 6 long gates. On *ibm_sherbrooke*, longer gate durations have a strong impact, with EPLG increasing from 1.9×10^{-2} to 3.7×10^{-2} (95% higher). On $ibm_marrakesh$, the effect is minimal, with EPLG increasing from 3.55×10^{-3} to 3.68×10^{-3} (4% higher) (see bottom of Fig. 5).

These results highlight that longer 2Q gate durations introduce significant variation on quantum devices, reinforcing the importance of considering these constraints.

5 Conclusion

In this work, we expand the analysis of the layer fidelity benchmark to enhance its applicability in device performance evaluation. We introduced a protocol for identifying optimal qubit chains of length N, demonstrating that our approach yields EPLG values 40-70% lower than those from randomly selected chains. While the one-dimensional chain used here was selected for it's versatility—it is amenable to many device topologies, easily scaled in size and well-suited for depth free search—the overall approach can be readily generalized to other layer fidelity topologies. For instance, a square layer (4 disjoint layers) could be adopted for processors with a four-nearest-neighbor square topology, such as the planned IBM Nighthawk processor. Nonetheless, the chain remains a valuable construct, as it provides a simple yet effective means of capturing device performance trends. By tracking layer fidelity over time, we also established EPLG as an effective stability monitoring tool, capable of detecting both localized and devicewide performance degradations. Additionally, we refined the accuracy of RB decay fits, determining reasonable bounds on the number of randomizations and Clifford lengths to minimize fit uncertainties. Our results show that six or more randomizations provide stable EPLG estimates, while a minimal number of 300 Cliffords is necessary. Finally, we analyzed the impact of gate duration constraints on layer fidelity measurements. We found that longer 2Q gate durations significantly increase layered gate errors on Eagle R3 processors, with EPLG rising by 95% when gate durations were extended by 65%. These findings refine the use of layer fidelity as a quantum benchmarking tool.

6 Acknowledgments

The authors would like to thank Youngseok Kim, Luke Govia and Seth Merkel for insightful discussions. We also want to thank Oliver Dial for writing a holistic depth-first-search algorithm for finding the best qubitchain on a device. Research was partially supported by the Army Research Office and was accomplished under Grant Number W911NF-21-1-0002. The views and conclusions contained in this document are those of the authors and should not be interpreted as representing the official policies, either expressed or implied, of the Army Research Office or the U.S. Government. The U.S. Government is authorized to reproduce and distribute reprints for Government purposes notwith-standing any copyright notation herein.

References

- [1] S. Boixo, S. V. Isakov, V. N. Smelyanskiy, R. Babbush, N. Ding, Z. Jiang, M. J. Bremner, J. M. Martinis, and H. Neven. Characterizing quantum supremacy in near-term devices. *Nature Physics* 14, 595, 2018.
- [2] J. Burnett, L. Faoro, and I. Wisby. Evidence for interacting two-level systems from the 1/f noise of a superconducting resonator. Nat Commun 5, 4119, 2014
- [3] J. M. Chow, A. D. Córcoles, J. M. Gambetta, C. Rigetti, B. R. Johnson, J. A. Smolin, J. R. Rozen, G. A. Keefe, M. B. Rothwell, M. B. Ketchen, and M. Steffen. Simple all-microwave entangling gate for fixed-frequency superconducting qubits. *Phys. Rev. Lett.*, 107:080502, Aug 2011.
- [4] A. W. Cross, L. S. Bishop, S. Sheldon, P. D. Nation, and J. M. Gambetta. Validating quantum computers using randomized model circuits. *Physical Review A* 100, 032328, 2019.
- [5] A. M. Dalzell, S. McArdle, M. Berta, P. Bienias, C.F. Chen, A. Gily'en, C. T. Hann, M. J. Kastoryano, E. T. Khabiboulline, A. Kubica, G. Salton, S. Wang, and F. G. S. L. Brandao. Quantum algorithms: A survey of applications and end-toend complexities, arxiv preprint. arXiv:2310.03011 [quant-ph], 2023.
- [6] L. Faoro and L. B. Ioffe. Internal loss of superconducting resonators induced by interacting two-level systems. *Phys. Rev. Lett.*, 109:157005, 2012.
- [7] S. Ferracin, A. Hashim, J.-L. Ville, R. Naik, A. Carignan-Dugas, H. Qassim, A. Morvan, D. I.

- Santiago, I. Siddiqi, and J. J. Wallman. Efficiently improving the performance of noisy quantum computers, arxiv preprint. arXiv:2201.10672 [quant-ph], 2022.
- [8] J. M. Gambetta. The hardware and software for the era of quantum utility is here — ibm quantum computing blog, 2023. Accessed: Feb. 10, 2025.
- [9] J. M. Gambetta, A. D. C'orcoles, S. T. Merkel, B. R. Johnson, J. A. Smolin, J. M. Chow, C. A. Ryan, C. Rigetti, S. Poletto, T. A. Ohki, M. B. Ketchen, and M. Steffen. Characterization of addressability by simultaneous randomized benchmarking. Phys. Rev. Lett. 109, 240504, 2012.
- [10] J. M. Gambetta and R. Mandelbaum. Ibm quantum delivers on 100x100 challenge ibm quantum computing blog, 2024. Accessed: Feb. 10, 2025.
- [11] J. Helsen, I. Roth, E. Onorati, A. Werner, and J. Eisert. General framework for randomized benchmarking. PRX Quantum 3, 020357, 2022.
- [12] J. Hines, D. Hothem, R. Blume-Kohout, B. Whaley, and T. Proctor. Fully scalable randomized benchmarking without motion reversal, arxiv preprint. arXiv:2309.05147 [quant-ph], 2023.
- [13] A. Kandala, K. X. Wei, S. Srinivasan, E. Magesan, S. Carnevale, G. A. Keefe, D. Klaus, O. Dial, and D. C. McKay. Demonstration of a high-fidelity cnot gate for fixed-frequency transmons with engineered zz suppression. *Phys. Rev. Lett.*, 127:130501, Sep 2021.
- [14] Y. Kim, A. Eddins, S. Anand, K. X. Wei, E. Van Den Berg, S. Rosenblatt, H. Nayfeh, Y. Wu, M. Zaletel, K. Temme, and A. Kandala. Evidence for the utility of quantum computing before fault tolerance. *Nature* 618, 500, 2023.
- [15] Y. Kim, L. C. G. Govia, A. Dane, E. van den Berg, D. M. Zajac, B. Mitchell, Y. Liu, K. Balakrishnan, G. Keefe, A. Stabile, E. Pritchett, J. Stehlik,

- and A. Kandala. Error mitigation with stabilized noise in superconducting quantum processors, arxiv preprint. arXiv:2407.02467 [quant-ph], 2024.
- [16] E. Magesan, J. M. Gambetta, and J. Emerson. Characterizing quantum gates via randomized benchmarking. *Phys. Rev. A* 85, 042311, 2012.
- [17] D. C. McKay, I. Hincks, E. J. Pritchett, M. Carroll, L. C. G. Govia, and S. T. Merkel. Benchmarking quantum processor performance at scale, arxiv preprint. arXiv: 2311.05933, 2023.
- [18] S. Merkel, T. Proctor, S. Ferracin, J. Hines, S. Barron, L. C. G. Govia, and D. C. McKay. When clifford benchmarks are sufficient; estimating application performance with scalable proxy circuits, arxiv preprint. arXiv:2503.05943, 2025.
- [19] C. Müller, J. Lisenfeld, A. Shnirman, and S. Poletto. Interacting two-level defects as sources of fluctuating high-frequency noise in superconducting circuits. *Phys. Rev. B*, 92:035442, 2015.
- [20] T. Proctor, S. Seritan, K. Rudinger, E. Nielsen, R. Blume-Kohout, and K. Young. Scalable randomized benchmarking of quantum computers using mirror circuits. *Phys. Rev. Lett.* 129, 150502, 2022.
- [21] T. J. Proctor, A. Carignan-Dugas, K. Rudinger, E. Nielsen, R. Blume-Kohout, and K. Young. Direct randomized benchmarking for multiqubit devices. *Phys. Rev. Lett.* 123, 030503, 2019.
- [22] S. Sheldon, E. Magesan, J. M. Chow, and J. M. Gambetta. Procedure for systematically tuning up cross-talk in the cross-resonance gate. *Phys. Rev. A*, 93:060302, Jun 2016.
- [23] E. v. d. Berg, Z. K. Minev, A. Kandala, and K. Temme. Probabilistic error cancellation with sparse pauli-lindblad models on noisy quantum processors, arxiv preprint. arXiv:2201.09866, 2022.